Adapted Generalized Unsharp Masking Algorithm for Sharpness Improvement of Scanning Electron Microscopy Images

Zaid Natiq Alsaygh, Zohair Al-Ameen

Department of Computer Science, College of Computer Science and Mathematics, University of Mosul, Nineveh, Iraq

ARTICLE INFO

ABSTRACT

The scanning electron microscope (SEM) images are highly valuable in different scientific applications because they can depict extremely small entities. SEM images are sometimes obtained blurry, in that such an issue reduces the clarity and hampers the detection of important features in the image. One way of processing the unwanted blurring effect is to use image sharpening, which aims at emphasizing the edges so that the output appears more significant to the observer with better-highlighted details. Many image sharpening methods exist, but not all are efficient as they may introduce artifacts, unnatural appearance, contrast/brightness modifications, or can be complicated and require a high computational cost. One algorithm of interest is the generalized unsharp mask (GUSM), which avoids the generation of artifacts that many sharpening methods own and have a somewhat simple structure. Still, when the GUSM algorithm is applied to different SEM images, it provides an unnatural sharpness and modifies the contrast and brightness as well. This is undesirable because proper sharpening is required for SEM images as they depict important information. Hence, an adapted GUSM algorithm is introduced in this article, in that it provides a more natural sharpening without modifying the brightness or contrast of the filtered images. The main contribution of this study is to remove the contrast enhancement procedure and replace the smoothing process to deliver more natural sharpness. The developed AGUSM algorithm is verified with different real-unclear SEM images, its performance is appraised against different image sharpening methods, and the outcomes of comparisons are evaluated by utilizing advanced metrics. For the performed experiments, the AGUSM provided satisfying performances as the outcomes appear to have more acutance and looked more natural when compared to the original counterparts and the outcomes of the comparison methods.

Corresponding Author:

Zohair Al-Ameen, Department of Computer Science, College of Computer Science and Mathematics, University of Mosul, Nineveh, Iraq
Email: qizohair@uomosul.edu.iq

1. INTRODUCTION

The scanning electron microscope (SEM) has provided tremendous services for many scientific fields due to its incredible capabilities in viewing the tiny structures of the scanned surfaces [1, 36]. SEM devices enabled the acquirement of amazing details of the micro and nanostructures that could not be seen by traditional microscopes [2, 37]. SEM devices generally work by concentrating a high-energy beam of electrons on a surface to obtain a digital image [3, 38]. This means that SEM images are the result of interaction between the scanned surface and the beam of electrons, in that the quality of the output image is somewhat controlled by the size of the beam [4]. Traditional microscopes can magnify surfaces up to one thousand five hundred times, while the SEM can magnify surfaces up to thirty thousand times [5]. SEM images are obtained in a grayscale form and can be colorized by employing a specialized approach for better representation [6].

Despite the major advancement that SEM devices have reached, it still generates images with artifacts, wherein such images must be processed efficiently so that the results are artifacts-free, clear, and more accurate [7]. The blur is one of the most well-known and common digital image artifacts, as it drastically lowers the visual quality of an image, making it difficult to correctly notice its small features [8]. Blur happens in SEM devices for many reasons [33] including electron scattering [30], beam deflection [31], improper focus [32], and low-beam energy [34], and imaging errors [35]. Sharpness is the opposite of blurring, and it is the key feature that makes an image appear more visually pleasing to the observer [10, 39]. One way to reduce the blurring effect is to use a proper image sharpening method, as different image sharpening approaches have been introduced for such purposes and are thoroughly examined in Section 2. The main aim of image sharpening is to increase the acutance of important details without introducing unwanted distortions [9, 40]. In addition, the main goal of this research is to improve the acutance of SEM images without introducing any errors to the processed images.

Different image sharpening methods have been studied and the generalized unsharp mask (GUSM) method is selected because it avoids the generation of the unwanted artifacts that the traditional sharpening methods produce. Still, The GUSM modifies the contrast and produces unnatural sharpness when applied to different SEM images. Hence, an adapted GUSM algorithm is presented to deliver more natural sharpening without modifying the image brightness or contrast. The main contribution of this study is modifying the algorithm by removing the contrast enhancement process and replacing the smoothing process with a better one to deliver more natural sharpening to the processed images. Many tests and comparisons are made to show the efficiency of the proposed algorithm. The study organization goes as follows: Section 2 contains a thorough review of the relevant literature; Section 3 includes a full explanation of the proposed algorithm; Section 4 contains a description of the needed experiments, comparisons, and their analysis; Section 5 includes a summary of important concluding remarks.

2. RELATED WORK

Many concepts for image sharpening have been introduced in the past years, but each one has its advantages and disadvantages. Kim and Allebach [11] suggested an ideal unsharp mask filter that works by applying a pixel classification using a Laplacian of Gaussian operator. Next, the output is processed by a high-pass filter, and the result is combined with the original image to generate the result. Millán and Valencia [12] suggest a human visual model-based method. It utilizes the concept of viewing distance, spatial filters, and the Laplacian of Gaussian to produce the resulting image. This can be achieved by inferring changes in the original image at short viewing distances, where the spatial opacity is low, and sharpening most fine edges and object contour lines with thin double edges. Large objects are sharpened solely by adding thick double edges at long distances, where the spatial opacity is larger.

Gui and Liu [13] proposed a fuzzy logic-based method. It works by finding the difference between the central pixel's value and the values of the eight neighboring pixels, wherein the sharpness is proportional to the difference, where the greater the difference, the lower the intensity. Skoneczny [14] introduced a pseudo-top-hat transformation-based algorithm. It works by applying pseudo-top-hat transforms of the dark and bright areas of the image separately. Then, the contrast operator is obtained based on the aforesaid transforms using a specialized approach. Finally, a lexicographical-based approach is applied to create the output image. Yang [15] proposed a masking coefficients-based algorithm. It works by applying four distinct masking coefficients in four different directions to magnify the high-frequency (HF) information. Then, a nonlinear transfer method is applied to filter the HF information and produce a sharp image.

Pham and Jeon [16] developed adaptive guided filtering (AGF)-based algorithm. It works by computing the AGF filter to properly determine an offset image. Next, different local statistics are determined from the original, AGF, and offset images. Finally, the sharpened image is created by using a specialized linear transformation method. Zafeiridis et al. [17] introduced a wavelet-based fusion algorithm. It works by processing the input by a 2D dual-tree discrete wavelet transform approach. Next, five dissimilar sharpening approaches are implemented. Finally, a specialized image fusion method is implemented to get the sharpened output. Zerbino [18] provided an algorithm that depends on neural networks and cellular automata. It works by filtering the input by a logical filter which utilizes the concept of the neural network to analyze the small logical components of the image. Next, the cellular automata concept is applied to improve the sharpness of the small image details.

Luo et al [19] developed an information entropy-based algorithm. It works by computing the information entropy of the segmented input image. Next, a specialized threshold by utilizing an adaptive entropy-based entropy algorithm. Then, the image segment that owns an entropy less than the threshold is sharpened and the overall image is created. Huang [9] introduced a green function-based algorithm. It works by mapping image

features to a Poisson equation and a retinex model. Then, adaptive processing is implemented to modify the features and create the output image. As given in the reviewed methods above, different concepts have been utilized for image sharpening. A synopsis is given in table 1 to summarize the reviewed methods. Accordingly, not all methods have been successful in this task, as some have excessive computations and others produce artifacts, unnatural sharpness, or inadequate enhancement. Thus, developing an algorithm that can produce adequate results is desirable and the door remains open for such a task to be attained.

Table 1. Synopsis of the reviewed methods.

#	Author & Year	Concept	Intricacy	Pros	Cons
1	(Kim and Allebach, 2005) [11]	Ideal unsharp masking	High	No noise amplification	Many computations
2	(Millán and Valencia, 2006) [12]	Human visual model	High	Considers the viewing distance	Noise may sharpen in some cases
3	(Gui and Liu, 2011) [13]	Fuzzy logic	Low	Simple computations	Does not provide enough enhancement
4	(Skoneczny, 2012) [14]	Top-hat transforms	Moderate	Makes the dark regions more visible	Brightness amplification
5	(Yang, 2014) [15]	Masking coefficients	Low	Non-complex method	Needs further improvements
6	(Pham and Jeon, 2015) [16]	Adaptive guided filtering with linear transformation	Moderate	Simple structure	Does not provide enough enhancement
7	(Zafeiridis et al., 2016) [17]	Wavelets and image fusion	High	Good sharpness improvement	Many computations
8	(Zerbino, 2019) [18]	Neural networks and cellular automata	High	Can sharpen different types of images	Blocking artifact
9	(Luo et al., 2020) [19]	Information entropy	Moderate	Balanced sharpening	Needs further improvements
10	(Huang, 2021) [9]	Green function	High	Good sharpness	Many computations

3. PROPOSED ALGORITHM

Image sharpening has been done in many ways as seen from the reviewed methods. One way of doing so is by using a generalized approach. In [20], a generalized unsharp masking approach has been introduced. This approach is used for sharpening and contrast enhancement. It uses different logarithmic processing of addition, subtraction, and multiplication to sharpen the image without introducing the over or under-shoot effect that is introduced by the standard unsharp masking method. This method starts by filtering the input image with a median filter to smooth the image and preserve its details simultaneously. This approach reduced the overshoot effect produced by the classical unsharp mask. Next, the ratios of the negative visions of the input image and its smoothed version are computed using the log-ratio notion by the following equations:

$$X_{(i,j)} = \frac{1 - W_{(i,j)}}{max(W_{(i,j)}, 0.01)} \tag{1}$$

$$Y_{(i,j)} = \frac{1 - F_{(i,j)}}{max(F_{(i,j)}, 0.01)} \tag{2}$$

where, $W_{i,j}$ is the original input image, $X_{i,j}$ is the negative of $W_{i,j}$, $F_{i,j}$ is image $W_{i,j}$ which is smoothed by the median filter, $Y_{i,j}$ is the negative of $F_{i,j}$, i and j are image coordinates. The image can be decomposed into parts, the first being the low-frequency which represents the scale of intensity (root signal) and the second being the high-frequency which represents the residual (details signal). Accordingly, the details signal is computed, in that it contains information about the noticeable details of the image. The details signal is computed using a generalized subtraction procedure as follows:

$$D_{(i,j)} = \frac{1}{\left(1 + \left(\frac{X_{(i,j)}}{Y_{(i,j)}}\right)\right)} \tag{3}$$

where, $D_{i,j}$ is the details signal that will be sharpened from the image. After that, image $F_{i,j}$ is used again and filtered by the contrast limited adaptive histogram equalization (CLAHE) approach to modify its contrast and to be used later to modify the contrast of the sharpened image, in that the output of this step is $H_{i,j}$. The details signal must be controlled by a certain gain to get the desirable results. when using a general gain, adequate results cannot be obtained because large gain values must be used in this case to enhance the small details, and this can lead to information loss. Thus, adaptive can must be utilized in this case to enhance the details appropriately. Hence, an adaptive gain control (AGC) approach using log-ratio procedures is utilized to solve this problem. The AGC approach starts by conducting a linear mapping procedure on the details signal $D_{i,j}$ to get a new signal $C_{i,j}$ as follows:

$$C_{(i,j)} = \left(2D_{(i,j)}\right) - 1 \tag{4}$$

In that, the interval of $C_{i,j}$ is (-1,1). After that, the gain is made as a function of $C_{i,j}$ to perform a gradual decrease for the gain from its highest value to the lowest value when $|C_{i,j}| \rightarrow 1$. This can be achieved using the following adaptive gain approach:

$$\gamma\left(C_{(i,j)}\right) = \alpha + \beta \, exp\left(-\left|C_{(i,j)}\right|^{\eta}\right) \tag{5}$$

where η represents a factor that regulates the reduction rate, α and β are the adaption factors that are computed using the following equations:

$$\beta = \frac{\gamma_{MAX} - \gamma_{MIN}}{1 - \exp(-1)} \tag{6}$$

$$\alpha = \gamma_{MAX} \tag{7}$$

To get a significant AGC effect, the setting is made as follows: $\gamma_{MAX} = 5$, $\gamma_{MIN} = 1$, and $\eta = 0.5$. As for $\gamma_{MIN} = 1$, this situation is appropriate for not providing more amplification when the value in the details signal is large. As for $\gamma_{MAX} = 5$, it aids to improve the smallest image detail.

Now, the AGC should be applied to the details signal to sharpen the image. This can be done using the addition operation of the log-ratio process as follows:

$$R_{(i,j)} = \frac{1}{max\left(0.1, \left(1 + \frac{1 - G_{(i,j)}}{max\left(G_{(i,j)}, 0.01\right)} \frac{1 - H_{(i,j)}}{max\left(H_{(i,j)}, 0.01\right)}\right)\right)} \tag{8}$$

$$G_{(i,j)} = \frac{1}{\left(1 + Q_{(i,j)}^{\gamma\left(c_{(i,j)}\right)}\right)} \tag{9}$$

$$Q_{(i,j)} = \frac{\left(1 - D_{(i,j)}\right)}{max\left(Q_{(i,j)}, 0,01\right)} \tag{10}$$

The final filtered output $R_{i,j}$ represents an image with improved sharpness and contrast. As this algorithm is tested with different images, contrast enhancement is not always needed with image sharpening. Likewise, the used CLAHE approach may not be appropriate for different types of images as it is a legacy method that have been developed in 1987 [21]. Moreover, the sharpness of the output needs to appear more natural as some images appeared with unusual sharpness. Fig. 1 demonstrates the block diagram of the original GUSM algorithm.

Hence, improving this method remains possible as it does not introduce the classical artifacts of the traditional unsharp mask filter as well as, and it owns a simple structure with a non-iterative nature. The modifications that are made to this algorithm are as follows: firstly, instead of using the median filter to smooth the input image, the classical bilateral filter is used instead as it provides more natural sharpening when utilized with this algorithm. Secondly, the use of CLAHE has been avoided, so that the GUSM can be used for image sharpening only. In the beginning, the bilateral filer was introduced in [22] under the name of SUSAN, then later was named bilateral in [23].
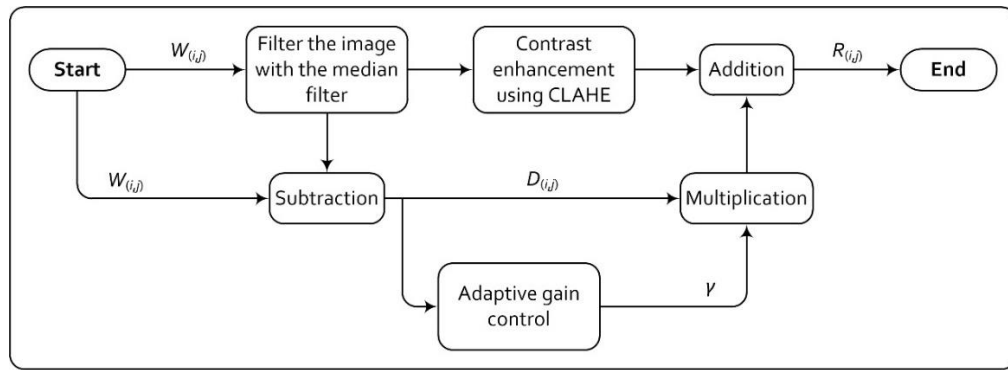
Fig. 1. The diagram of the original GUSM algorithm.

Due to its acceptable performance and low computations, it became one of the well-known filters in the field of image smoothing. Its main aim is to attenuate the frequencies that are deemed high by weighting and averaging in a nonlinear way. It processes the high-leveled intensities in different variations to maintain well-defined edges while smoothing the image. This can be achieved by conducting a fine-similarity choice between two given pixels via the check of the spatial distance (SD), in that it checks the similarity of pixels' intensities and the sufficiency of their SD. Suppose that the original unprocessed image is $W_{i,j}$ and its processed version is $F_{i,j}$, (m and n) are pixel coordinates, the bilateral filter can be computed as follows [23]:

$$F_{(i,j)} = \frac{\sum G_{(m,n)} W_{(m,n)}}{\sum G_{(m,n)}} \tag{11}$$

where, $G_{(m,n)}$ represents the mask of the total weight (MTW). The MTW is computed using the following equation:

$$G_{(m,n)} = \left[exp \left(- \frac{(m-i)^2 + (n-j)^2}{2\sigma_s^2} \right) \right] \cdot \left[exp \left(- \frac{\left[W_{(m,n)} - W_{(i,j)} \right]^2}{2\sigma_r^2} \right) \right] \tag{12}$$

where σ_s and σ_r are the standard derivations that describe the kernel of the gaussian. In this study, the size of the kernel is equal to 8×8, $\sigma_r = 0.2$, $\sigma_s = 8$. The output $F_{i,j}$ is used instead of the one produced by the original GUSM. As for CLAHE, it has been removed from the algorithm, and in this case, $H_{i,j} = F_{i,j}$ in equation 8. To clearly understand the proposed algorithm, Fig. 2 is provided, which demonstrates the block diagram of the proposed AGUSM.
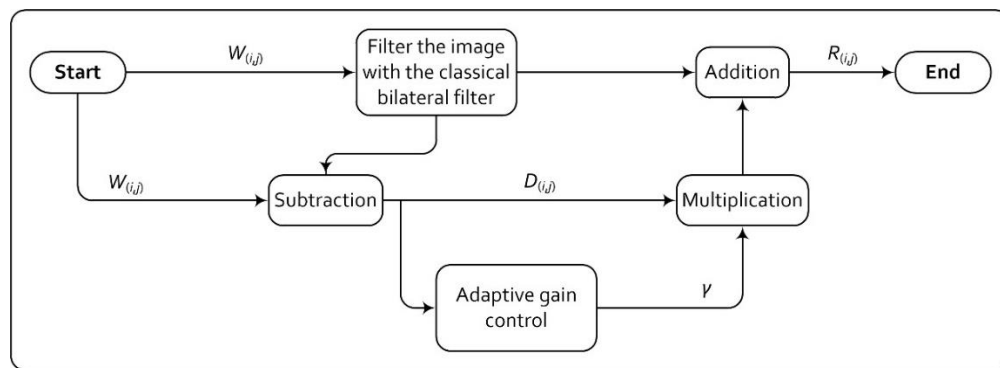

Fig. 2. The diagram of the proposed AGUSM algorithm.

4. RESULTS AND DISCUSSION

The results of comparisons, tests, and relevant analysis are given in this section. The dataset of images was collected from different sources online as nearly 200 natural-blurred images were collected, all of them are grayscale and range in size from 500×500 to 3000×3000 pixels. Four websites were mainly used to collect the dataset, these websites are dartmouth.edu, ualberta.ca, consistence.nl/gallery/, and particletechlabs.com. For adequate image utilization, the collected images are categorized, numbered, and in some cases cropped.

The proposed work is compared with several known image sharpening methods to genuinely quantify the processing ability of the proposed algorithm. The comparison methods are the following: shock filter (SF) [24], GUSM [20], an eight-neighborhood operator sharpening (ENOS) [13], kernel-based sharpening (KBS) [25], modified Laplacian sharpening (MLS) [26], nonlinear unsharp masking (NUSM) [27].

Accordingly, the quality of the comparison outcomes is appraised using two no-reference image evaluation methods, namely the blur metric [28] and the maximum local variation (MLV) metric [29]. The blur metric analysis the change between the adjacent pixels by computing the intensity variation between those pixels. Next, a low-pass filter is applied to the same image to compute the fluctuation in intensity between the two image versions. The output is a numerical value, in that a higher value indicates better sharpness. As for the MLV metric, the MLV is determined for each pixel depending on its adjacent pixels. Next, the standard derivation of the MLV distribution is determined to produce the final score. The outcome of this metric is also a numerical value, in that a smaller value indicates a more natural-looking image.

The computer used in the experiments in this study is equipped with an Intel Core I3-2328M 2.20 GHz CPU and 4 GB of RAM. As for the programming environment, MATLAB 2018a is used for all experiments and comparisons. Fig. 3 to Fig. 5 demonstrate different empirical results of the proposed algorithm with various natural-blurred images. Fig. 6 to Fig. 9 illustrate the comparison results. Tables 2 to Tables 4 represent the obtained evaluation readings and runtimes. Fig. 10 to Fig. 12 depict the average scores of Tables 2 to Tables 4 as graphical charts.
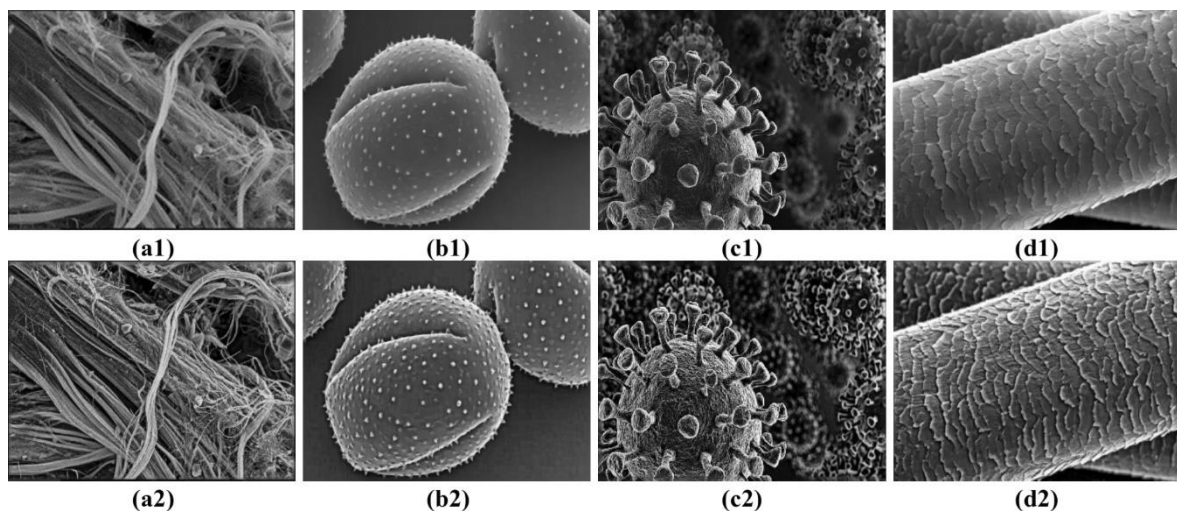

Fig. 3. Results obtained by the proposed AGUSM (Set -1-). (a1–d1) natural-blurred SEM images; (a2–d2) images processed by AGUSM with η = 0.5, 0.6, 0.7 and 0.8, respectively.
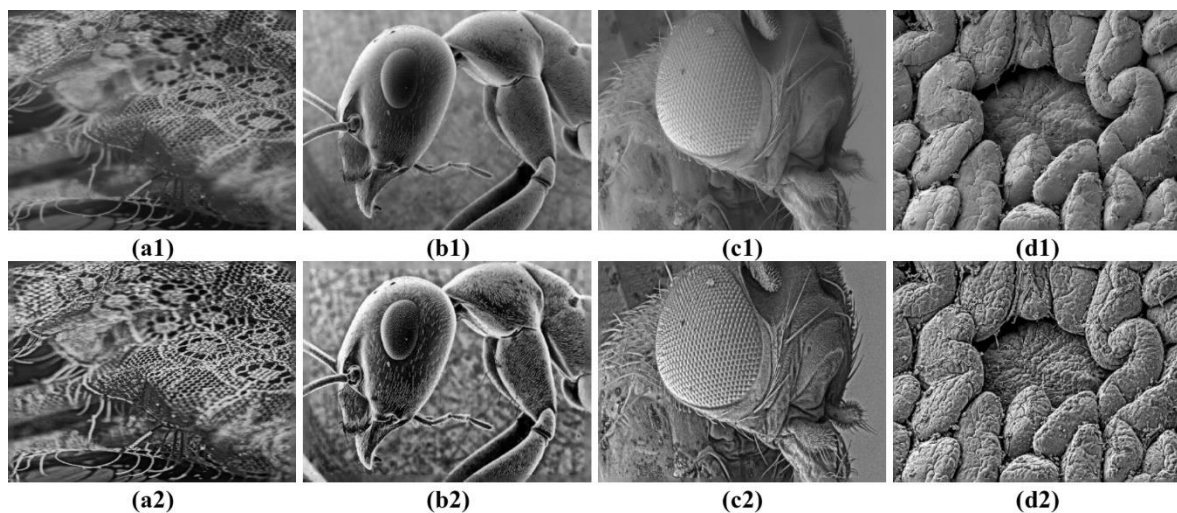

Fig. 4. Results obtained by the proposed AGUSM (Set -2-). (a1–d1) natural-blurred SEM images; (a2–d2) images processed by AGUSM with η = 0.55, 0.59, 0.65 and 0.69, respectively.
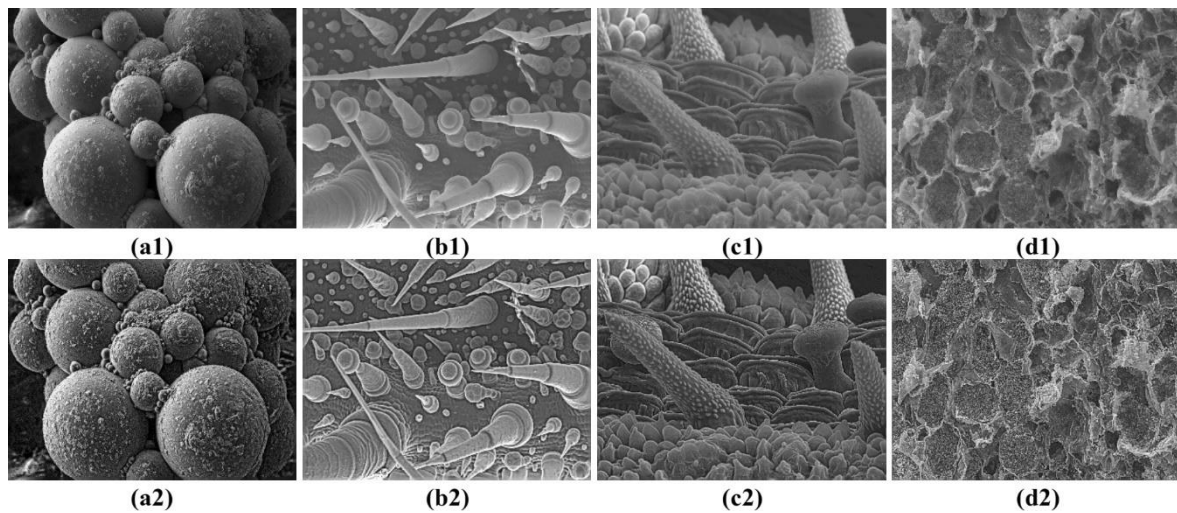
Fig. 5. Results obtained by the proposed AGUSM (Set -3-). (a1–d1) natural-blurred SEM images; (a2–d2) images processed by AGUSM with η = 0.95, 0.97, 0.99 and 1.3, respectively.

From Fig. 3 to Fig. 5, the results are obvious as they indicate that the proposed algorithm performed well and produced acceptable quality results in terms of acutance and naturalness. The outputs have better sharpness, natural appearance, better visual details, no processing flaws, and the intensity remains well-preserved. When comparing the unprocessed images with their processed versions, the difference is obvious as the results appear much better in detail. The value of η controls the sharpness amount in that a higher value leads to a more sharpening effect on the processed image.

From Fig. 6 to Fig. 12 and Table 2 to Table 4, the results are dissimilar as the notions are different. The MLS approach provided results with low sharpens and slight noise amplification, and it is ranked 7th with the blur metric, 4th with MLV, and 4th fastest method. This indicates that the sharpness has slightly increased and the naturality has become better.
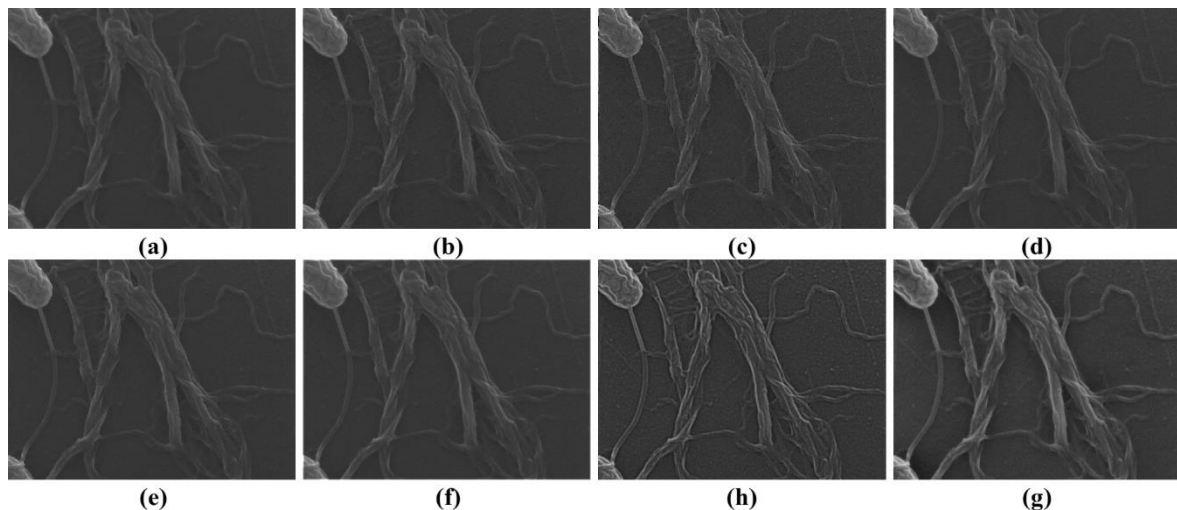

Fig. 6. The comparison results using a natural-blurred SEM image (Set -1-). (a) Original SEM image; images from (b–h) are processed by: (b) MLS, (c) ENOS, (d) KBS, (e) SF, (f) NUSM, (g) GUSM, (h) Proposed AGUSM.

The ENOS approach provided results with high noise amplification, and it is ranked 3rd with the blur metric, 7th with MLV, and 2nd fastest method. This indicates that the sharpness has increased but the naturality has been distorted due to the noise artifact. The KBS approach provided results with some noise amplification and acceptable acutance, and it is ranked 2nd with the blur metric, 6th with MLV, and it is the fastest method. This indicates that the sharpness has improved noticeably but the naturality has been reduced due to the noise artifact.

The SF approach provided results with a cartoon-like artifact, and it is ranked 6th with the blur metric, 5th with MLV, and 5th fastest method. This indicates that the perceived quality of the output image has been affected by the artifact generation although this approach showed the ability to increase the acutance of important details. The NUSM approach provided results with slight natural sharpness, and it is ranked 4th with the blur metric, 2nd with MLV, and 6th fastest method. This indicates that the sharpness has marginally increased in a way that the naturality has become significantly better.

The GUSM approach provided results with contrast modification and insufficient acutance, and it is ranked 5th with the blur metric, 3rd with MLV, and 3rd fastest method. This indicates that the sharpness has somewhat improved as well as its naturality has reached a somewhat acceptable level. The proposed AGUSM approach performed the best in terms of sharpness and naturality, as it is ranked the best with the blur and MLV metrics while being the slowest method. The outcomes of AGUSM own a much more natural sharpness and the details stood out better and the noise has been suppressed. The drawback of AGUSM is that it required a somewhat long time to implement due to the use of the bilateral filter, which requires some time to complete its filtering. Despite that, acceptable results have been attained and the overall quality is satisfactory. Developing an image sharpening algorithm is uneasy due to artifact generation and the research topic itself being uneasy. Yet, the development is made, and adequate results have been attained.
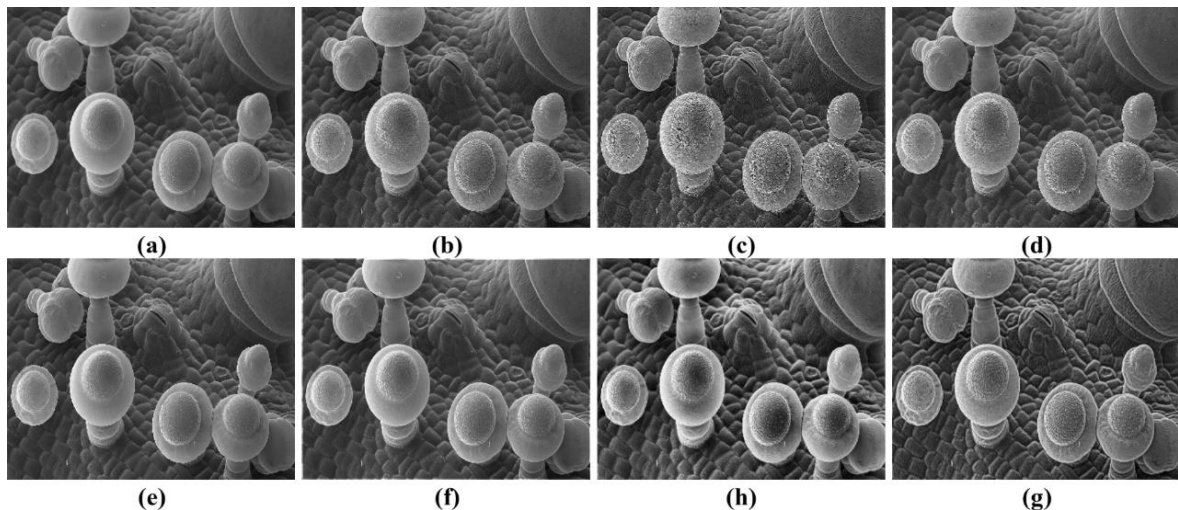

Fig. 7. The comparison results using a natural-blurred SEM image (Set -2-). (a) Original SEM image; images from (b–h) are processed by: (b) MLS, (c) ENOS, (d) KBS, (e) SF, (f) NUSM, (g) GUSM, (h) Proposed AGUSM.

Fig. 8. The comparison results using a natural-blurred SEM image (Set -3-). (a) Original SEM image; images from (b–h) are processed by: (b) MLS, (c) ENOS, (d) KBS, (e) SF, (f) NUSM, (g) GUSM, (h) Proposed AGUSM.
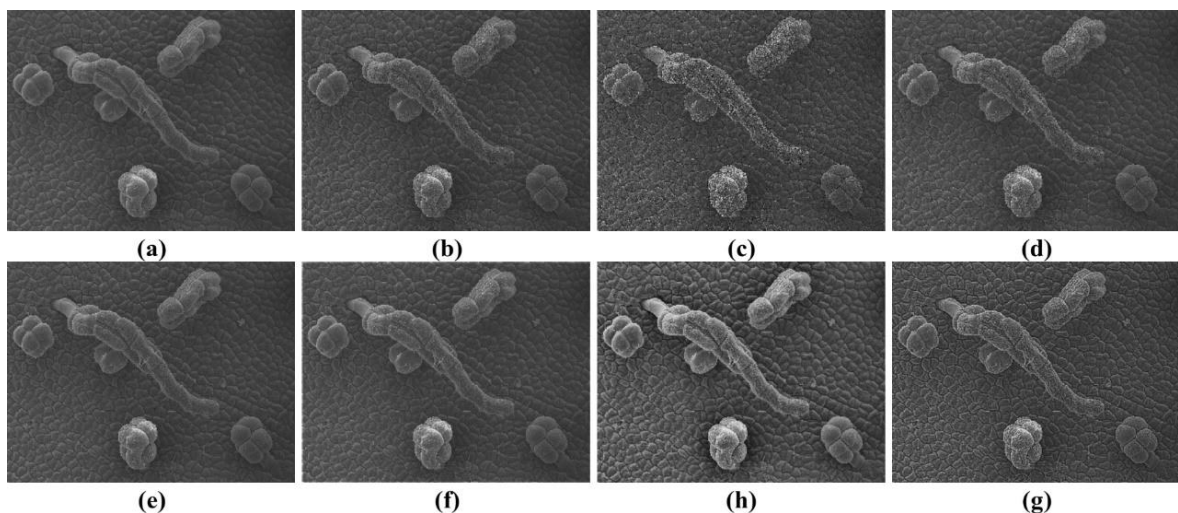
Fig. 9. The comparison results using a natural-blurred SEM image (Set -4-). (a) Original SEM image; images from (b–h) are processed by: (b) MLS, (c) ENOS, (d) KBS, (e) SF, (f) NUSM, (g) GUSM, (h) Proposed AGUSM.
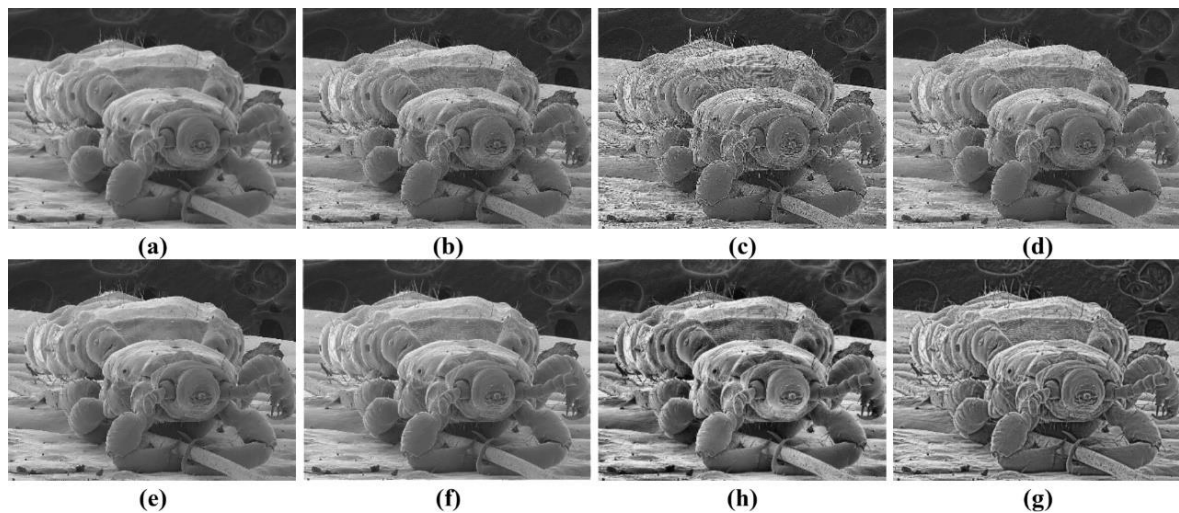
Table 2. The recorded accuracies of the blur metric.

Comparatives	Fig 6	Fig 7	Fig 8	Fig 9	Average
MLS	0.1692	0.1317	0.1281	0.1394	0.1421
ENOS	0.2546	0.2381	0.2647	0.234	0.24785
SF	0.2131	0.1456	0.1398	0.1412	0.159925
KBS	0.2804	0.2387	0.2709	0.2218	0.25295
NUSM	0.3018	0.2321	0.2552	0.2016	0.247675
GUSM	0.2599	0.215	0.2514	0.1923	0.22965
Proposed AGUSM	0.297	0.2322	0.2812	0.2064	0.2542

Table 3. The recorded accuracies of the MLV metric.

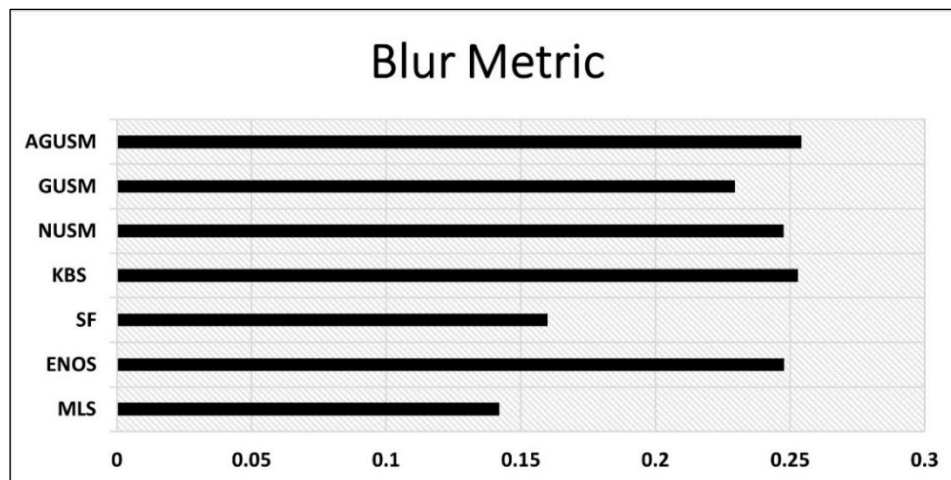| Comparatives	Fig 6	Fig 7	Fig 8	Fig 9	Average
MLS	0.0692	0.2224	0.2148	0.2198	0.18155
ENOS	0.1476	0.2225	0.2225	0.2225	0.203775
SF	0.1168	0.2223	0.173	0.2181	0.18255
KBS	0.0796	0.2225	0.2225	0.2225	0.186775
NUSM	0.1058	0.2075	0.1533	0.1663	0.158225
GUSM	0.0636	0.2163	0.1703	0.1855	0.158925
Proposed AGUSM	0.0706	0.2085	0.1668	0.1689	0.1537

Fig. 10. The average readings of the blur metric in Table 2.

Table 4. The application times (in seconds) for the comparison algorithms.

| Comparatives	Fig 6	Fig 7	Fig 8	Fig 9	Average
MLS	0.853027	0.200344	1.025363	0.174259	0.563248
ENOS	0.074356	0.093176	0.110614	0.088937	0.091771
SF	2.127098	0.981107	3.840486	0.865961	1.953663
KBS	0.076509	0.083095	0.097842	0.072242	0.082422
NUSM	2.198843	2.020084	8.225194	1.788152	3.558068
GUSM	0.378188	0.268502	1.088914	0.329059	0.516166
Proposed AGUSM	16.19873	13.386159	62.403376	11.458332	25.86164
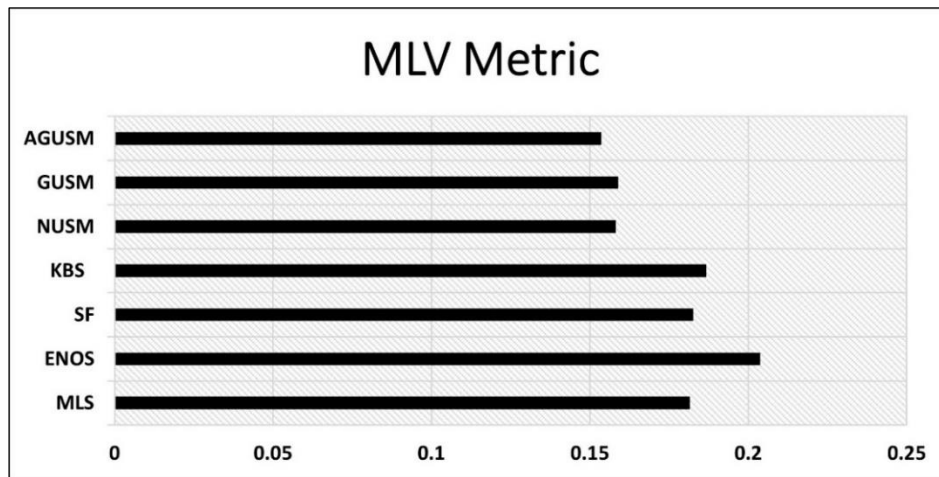
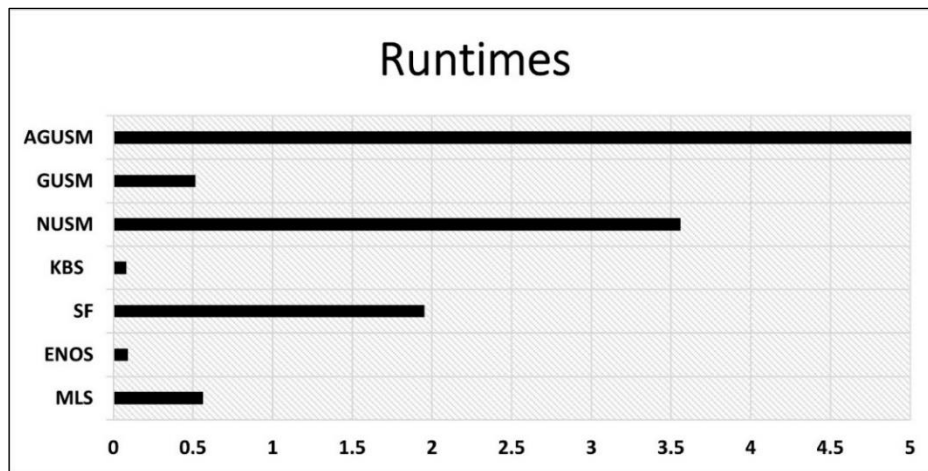**Fig. 11.** The average readings of the MLV metric in Table 3.

Fig. 12. The average runtimes of the comparison in Table 4.

5. CONCLUSION

In this study, an adapted GUSM algorithm is developed for SEM images. The adaption includes removing the contrast enhancement step and changing the smoothing filter to a more robust one to deliver a more realistic sharpening procedure. A dataset set of more than two hundred real-distorted SEM images is used in this study for comparisons and experiments to know the exact effects of the sharpening capability of the proposed algorithm. Different experiments, comparisons, and accuracy measurements were performed, and the outcomes are promising. By looking at the results, the proposed AGUSM algorithm delivered satisfying performances as the results are observed better and appeared clearer with no artifacts. This is reflected in the comparison results as well as the AGUSM provided the best accuracy and sharpness naturality as indicated by the obtained results and the metrics readings. In the future, this algorithm can be further improved by using a low complexity yet efficient smoothing filter that makes the sharpening more natural.

REFERENCES

[1] M. Ali et al., "Pollen micromorphology of eastern Chinese Polygonatum and its role in taxonomy by using scanning electron microscopy," *Microscopy Research and Technique*, vol. 84, no. 7, pp. 1451–1461, 2021, https://doi.org/10.1002/jemt.23701.

[2] E. Pach and A. Verdaguer, "Studying ice with environmental scanning electron microscopy," *Molecules*, vol. 27, no. 1, p. 258, 2021, https://doi.org/10.3390/molecules27010258.

[3] M. A. Sutton, N. Li, D. C. Joy, A. P. Reynolds, and X. Li, "Scanning electron microscopy for quantitative small and large deformation measurements part I: SEM imaging at magnifications from 200 to 10,000," *Experimental Mechanics*, vol. 47, no. 6, pp. 775–787, 2007, https://doi.org/10.1007/s11340-007-9042-z.

[4] A. E. Vladár, M. T. Postek, and M. P. Davidson, "Image sharpness measurement in scanning electron microscopy-part II," *Scanning*, vol. 20, no. 1, pp. 24–34, 2006, https://doi.org/10.1002/sca.1998.4950200104.

[5] Z. Al-Ameen, "An improved contrast equalization technique for contrast enhancement in scanning electron microscopy images," *Microscopy Research and Technique*, vol. 81, no. 10, pp. 1132–1142, 2018, https://doi.org/10.1002/jemt.23100.

[6] K. Ohta, S. Sadayama, A. Togo, R. Higashi, R. Tanoue, and K.-I. Nakamura, "Beam deceleration for block-face scanning electron microscopy of embedded biological tissue," *Micron*, vol. 43, no. 5, pp. 612–620, 2012, https://doi.org/10.1016/j.micron.2011.11.001.

[7] M. E. Rudnaya, R. M. Mattheij, and J. M. L. Maubach, "Evaluating sharpness functions for automated scanning electron microscopy," *Journal of Microscopy*, vol. 240, no. 1, pp. 38–49, 2010, https://doi.org/10.1111/j.1365-2818.2010.03383.x.

[8] M. R. Banham and A. K. Katsaggelos, "Digital image restoration," *IEEE Signal Processing Magazine*, vol. 14, no. 2, pp. 24–41, 1997, https://doi.org/10.1109/79.581363.

[9] Q. Huang, "An image sharpness enhancement algorithm based on Green function," *Traitement Du Signal*, vol. 38, no. 2, pp. 513–519, 2021, https://doi.org/10.18280/ts.380231.

[10] L. Li, D. Wu, J. Wu, H. Li, W. Lin, and A. C. Kot, "Image sharpness assessment by sparse representation," *IEEE Transactions on Multimedia*, vol. 18, no. 6, pp. 1085–1097, 2016, https://doi.org/10.1109/TMM.2016.2545398.

[11] J. P. Allebach, "Optimal unsharp mask for image sharpening and noise removal," *Journal of Electronic Imaging*, vol. 14, no. 2, p. 023005, 2005, https://doi.org/10.1117/12.538366.

[12] M. S. Millán and E. Valencia, "Color image sharpening inspired by human vision models," *Applied Optics*, vol. 45, no. 29, pp. 7684–7697, 2006, https://doi.org/10.1364/AO.45.007684.

[13] Z. Gui and Y. Liu, "An image sharpening algorithm based on fuzzy logic," *Optik*, vol. 122, no. 8, pp. 697–702, 2011, https://doi.org/10.1016/j.ijleo.2010.05.010.

[14] S. Skoneczny, "Nonlinear image sharpening in the HSV color space," *Electrotechnical Review*, vol. 88, no. 2, pp. 140–44, 2012. http://pe.org.pl/articles/2012/2/39.pdf.

[15] C. C. Yang, "Finest image sharpening by use of the modified mask filter dealing with highest spatial frequencies," *Optik*, vol. 125, no. 8, pp. 1942–1944, 2014, https://doi.org/10.1016/j.ijleo.2013.09.070.

[16] C. C. Pham and J. W. Jeon, "Efficient image sharpening and denoising using adaptive guided image filtering," *IET Image Processing*, vol. 9, no. 1, pp. 71–79, 2015, https://doi.org/10.1049/iet-ipr.2013.0563.

[17] P. Zafeiridis, N. Papamarkos, S. Goumas, and I. Seimenis, "A new sharpening technique for medical images using wavelets and image fusion," *Journal of Engineering Science & Technology Review*, vol. 2016, no. 3, pp. 187–200, 2016, https://doi.org/10.25103/jestr.093.27.

[18] D. Zerbino, "Improving image sharpness by surface recognition," *Econtechmod: Scientific Journal*, vol. 4, no. 8, pp. 39–44, 2019, https://yadda.icm.edu.pl/baztech/element/bwmeta1.element.baztech-37477bd3-c190-4442-9520-0fd28b862646.

[19] K. Luo, M. Lin, P. Wang, S. Zhou, D. Yin, and H. Zhang, "Improved ORB-SLAM2 algorithm based on information entropy and image sharpening adjustment," *Mathematical Problems in Engineering*, vol. 2020, pp. 1–13, 2020, https://doi.org/10.1155/2020/4724310.

[20] G. Deng, "A generalized unsharp masking algorithm," *IEEE Transactions on Image Processing*, vol. 20, no. 5, pp. 1249–1261, 2011, https://doi.org/10.1109/TIP.2010.2092441.

[21] S. M. Pizer et al., "Adaptive histogram equalization and its variations," *Computer Vision, Graphics, and Image Processing*, vol. 39, no. 3, pp. 355–368, 1987, https://doi.org/10.1016/S0734-189X(87)80186-X.

[22] S. M. Smith and J. M. Brady, "SUSAN–a new approach to low level image processing," *International Journal of Computer Vision*, vol. 23, no. 1, pp. 45–78, 1997, https://doi.org/10.1023/A:1007963824710.

[23] C. Tomasi and R. Manduchi, "Bilateral filtering for gray and color images," in *Sixth International Conference on Computer Vision* (pp. 839-846), 1998, https://doi.org/10.1109/ICCV.1998.710815.

[24] S. Bettahar and A. B. Stambouli, "Shock filter coupled to curvature diffusion for image denoising and sharpening," *Image and Vision Computing*, vol. 26, no. 11, pp. 1481–1489, 2008, https://doi.org/10.1016/j.imavis.2008.02.010.

[25] Z. Al-Ameen, G. Sulong, and M. G. M. Johar, "Fast deblurring method for computed tomography medical images using a novel kernels set," *International Journal of Bio-Science and Bio-Technology*, vol. 4, no. 3, pp. 9–19, 2012, https://gvpress.com/journals/IJBSBT/vol4_no3/2.pdf.

[26] Z. Al-Ameen, S. Al-Ameen, and A. Al-Othman, "Improving the sharpness of digital images using a modified Laplacian sharpening technique," *IPTEK The Journal for Technology and Science*, vol. 29, no. 2, p. 44, 2019, https://doi.org/10.12962/j20882033.v29i2.3356.

[27] D. Ngo, S. Lee, and B. Kang, "Nonlinear unsharp masking algorithm," in *2020 International Conference on Electronics, Information, and Communication (ICEIC)*, 2020, https://doi.org/10.1109/ICEIC49074.2020.9051376.

[28] F. Crete, T. Dolmiere, P. Ladret, and M. Nicolas, "The blur effect: perception and estimation with a new no-reference perceptual blur metric," in *Human Vision and Electronic Imaging XII*, 2007, https://doi.org/10.1117/12.702790.

[29] K. Bahrami and A. C. Kot, "A fast approach for no-reference image sharpness assessment based on maximum local variation," *IEEE Signal Processing Letters*, vol. 21, no. 6, pp. 751–755, 2014, https://doi.org/10.1109/LSP.2014.2314487.

[30] Y. Ominami, K. Nakahira, S. Kawanishi, and S. Ito, "Reduction of electron scattering image blur for atmospheric scanning electron microscopy," *Microscopy and Microanalysis*, vol. 21, no. S3, pp. 241–242, 2015, https://doi.org/10.1017/S1431927615002007.

[31] L. Zhang, M. H. Garming, J. P. Hoogenboom, and P. Kruit, "Beam displacement and blur caused by fast electron beam deflection," *Ultramicroscopy*, vol. 211, p. 112925, 2020, https://doi.org/10.1016/j.ultramic.2019.112925.

[32] J. Na, G. Kim, S. H. Kang, S. J. Kim, and S. Lee, "Deep learning-based discriminative refocusing of scanning electron microscopy images for materials science," *Acta Materialia*, vol. 214, p. 116987, 2021, https://doi.org/10.1016/j.actamat.2021.116987.

[33] H. Morishita, T. Ohshima, M. Kuwahara, Y. Ose, and T. Agemura, "Resolution improvement of low-voltage scanning electron microscope by bright and monochromatic electron gun using negative electron affinity photocathode," *Journal of Applied Physics*, vol. 127, no. 16, p. 164902, 2020, https://doi.org/10.1063/5.0005714.

[34] M. Enyama, M. Sakakibara, S. Tanimoto, and H. Ohta, "Optical system for a multiple-beam scanning electron microscope," *Journal of Vacuum Science & Technology B*, vol. 32, no. 5, p. 051801, 2014, https://doi.org/10.1116/1.4891961.

[35] J. Na, G. Kim, S.-H. Kang, S.-J. Kim, and S. Lee, "Deep learning-based discriminative refocusing of scanning electron microscopy images for materials science," *Acta Materialia*, vol. 214, no. 116987, p. 116987, 2021, https://doi.org/10.1016/j.actamat.2021.116987.

[36] R. Laws, D. H. Steel, and N. Rajan, "Research techniques made simple: Volume scanning electron microscopy," *Journal of Investigative Dermatology*, vol. 142, no. 2, pp. 265-271.e1, 2022, https://doi.org/10.1016/j.jid.2021.10.020.

[37] K. L. House, L. Pan, D. M. O'Carroll, and S. Xu, "Applications of scanning electron microscopy and focused ion beam milling in dental research," *European Journal of Oral Sciences*, vol. 130, no. 2, p. e12853, 2022, https://doi.org/10.1111/eos.12853.

[38] R. Ali, K. El-Boubbou, and M. Boudjelal, "An easy, fast and inexpensive method of preparing a biological specimen for scanning electron microscopy (SEM)," *MethodsX*, vol. 8, no. 101521, p. 101521, 2021, https://doi.org/10.1016/j.mex.2021.101521.

[39] T. D. Pham, "Kriging-weighted laplacian kernels for grayscale image sharpening," *IEEE Access*, vol. 10, pp. 57094–57106, 2022, https://doi.org/10.1109/ACCESS.2022.3178607.

[40] R. Mankar, C. C. Gajjela, F. F. Shahraki, S. Prasad, D. Mayerich, and R. Reddy, "Multi-modal image sharpening in fourier transform infrared (FTIR) microscopy," *Analyst*, vol. 146, no. 15, pp. 4822–4834, 2021, https://doi.org/10.1039/D1AN00103E.